Heat-Resistant Ferritic-Martensitic Steel RUSFER-EK-181 (Fe-12Cr-2W-V-Ta-B) for Fusion Power Reactor

V.M.Chernov 1), M.V.Leontyeva-Smirnova 1), D.A.Blokhin 1), N.A.Degtyarev 1), A.G.Ioltukhovsky 1), E.M.Mozhanov 1), A.B.Sivak 2), T.M.Bulanova 3), A.E.Fedoseev 3), Z.E.Ostrovskiy 3), A.N.Tyumentsev 4), B.K.Kardashev 5), A.I.Blokhin 6), V.A.Romanov 6)

1) JSC "Bochvar Institute", 123098, Moscow, Russia
2) Kurchatov Institute, 123182, Moscow, Russia
3) JSC "Research Institute of Atomic Reactors", 433510, Dimitrovgrad, Russia
4) Tomsk State University, Tomsk, Russia
5) Ioffe Institute RAS, 194021, St-Petersburg, Russia
6) Leypunsky Institute, 249033, Obninsk, Russia

E-mail contact of main author: chernovv@bochvar.ru

Abstract. The study of initial and radiation physical-mechanical and nuclear-physical properties of Russian reduced activation ferritic-martensitic nanostructured steel RUSFER-EK-181 (RAFMS Fe-12Cr-2W-V-Ta-B) as advanced heat- and radiation-resistant structural material for fusion power reactors has been continued. The regularities of low temperature brittle fracture (crack growth resistance) of the steel at static and dynamic concentrated loads were investigated in the temperature range from -196 C to +100 C. The ductile-to-brittle transition temperatures (DBTT) were determined. The values of DBTT were in the range from -85 C to +35 C depending on the type of CVN-specimens and stress states (fatigue crack, central and side V-notches). The marked level of permanent deformation and impact toughness (not less than 3-5 J/cm^2) was observed at low temperatures (lower than DBTT). The results for the impact toughness of SM/ST specimens with different stress concentrators were compared to the fracture toughness. Short-term (yield strength, ultimate strength, elongation to rupture) and long-term (creep, diagram "stress vs. time to rupture") properties, temperature conductivity, thermal conductivity and linear expansion of the steel were investigated in the temperature range to 750 C Diffusion characteristics of self-point defects (vacancies and interstitial atoms) in iron crystal with dislocations of different types were calculated by the methods of multiscale modeling (kinetic Monte Carlo, anisotropic theory of elasticity) in the temperature range from room temperature to 1000 K. On the base of Russian nuclear complex ACDAM nuclear transmutation changes of the chemical composition of the steel were calculated for the long-term irradiation in neutron spectrum of the fusion reactor DEMO-RF (the project of "Kurchatov institute"). Obtained data for functional properties of the RAFMS RUSFER-EK-181 characterize it as the nanostructured structural steel with good heat resistance (up to 700 C), good resistance to low temperature embrittlement, sufficient radiation resistance of the chemical composition and the structure and phase state.

1. Introduction

Candidate structural materials for fusion power reactors include mainly reduced activation ferritic/martensitic steels (RAFMS) [1-3]. 12%Cr RAFMS are successful materials for the use for fusion and fast power reactors. The advantages are sufficient high-temperature strength, corrosion resistance, good thermo-physical behavior, and fast decay of radioactive inventory. These 12%Cr RAFMS steels have been optimized further towards long-term activation materials (impurities concentrations) and have been optimized further towards low temperature irradiation-induced embrittlement, and heat resistance.
The main RAFMS in the RF is the RAFMS RUSFER-EK-181 (Fe-12Cr-2W-V-Ta-B) [3-6]. RUSFER-EK-181 steel is related to precipitation hardening (nanostructured) materials type. In this paper the functional initial and radiation properties of the RUSFER-EK-181 has been continued. All the specimens were subjected to (1) the traditional (standard) thermal treatment (TTT) for ferritic-martensitic steels before tests – quenching from the temperature 1100 C, 1 hour, tempering at 720 C, 3 hour , and (2) new combined thermal treatment (CTT – additional cyclical treatment near the critical point of the "austenitic-ferritic" transition).

2. RUSFER-EK-181 Microstructure

Alloying by Cr-W-V-Ta-B under the certain C and N concentration relates RUSFER-EK-181 steel to ferrite-martensite class with percentage of δ-ferrite no more than 5%. Carbide phases precipitate during tempering with different compositions and sizes (Figs 1-2): M23C6, M6C, M3C, TaC, VC; Mean particle size (for sizes > 3 nm) is 75.1±7.4 nm (TEM). An important feature of the two-phase structure of the steel after TTT-treatment is the high density of nanoparticles with sizes lower than 5 nm uniformly distributed through the bulk of the material. These particles are interstitial phase based on vanadium carbonitride. In case of CTT- treatment the formation of nanosized particles is eliminated. This leads to the significant decrease of effects of dispersion and substructural strengthening and is the basic reason for decreasing of the strength of the steel after such treatment and is an important factor of lowering of the ductile-to-brittle transition temperature (fig. 7). Carbides provide precipitation hardening of the steel and fixation of low- and large-angle boundaries (grain boundary engineering).Selected composition and regimes of thermomechanical treatments put the steel into the class of dispersion hardening materials with good technological and mechanical properties in the temperature range (300-700) C. Impurity and alloying content (technological purity) provides fast induced activity decay of RUSFER-EK-181 steel. VC and M23C6 phases providing precipitation hardening of the steel after quenching and tempering. VC/TaC nanoparticles of 3–5 nm size providing precipitation hardening of the steel after quenching and tempering. VC/TaC nanoparticles of 3–5 nm size constitute an appreciable part of the carbide phase.

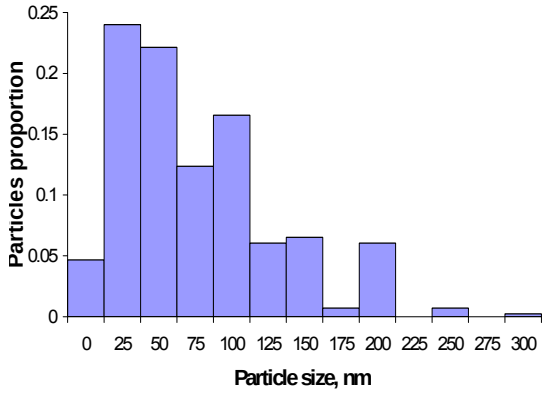

FIG. 1. Size distribution histograms of phases particles after air quenching and tempering.

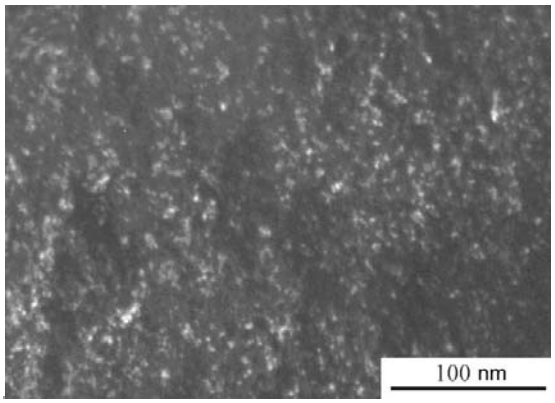

FIG. 2. Microstructure RUSFER-EK-181. VC/TaC and M23C6 of 3–5 nm size constitute an appreciable part of the carbide phase.

3. Fracture Toughness

The low temperature fracture behavior of the RAFMS RUSFER-EK-181 under impact and static concentrated bending loads have been investigated [6]. The dependence of fracture on the specimen size (standard and small), the type of stress concentrator (V-notch, fatigue crack) and temperature (from –196 C to +100 C) is determined. The ductile-to-brittle transition temperatures (DBTT) vary within the temperature range between -85 C and +35 C. The temperature dependence of the plane strain stress intensity factor K_{1C} and the fracture toughness J_{1C} is found. The most severe type of impact toughness test is a test of V-specimens sequentially augmented by a fatigue crack and two edge V-notches (three-sided V-notch with a central fatigue crack). The fracture energy depends on the type of stress concentrators and the specimen size. It depends on the amount of stored elastic energy and the conditions of plastic deformation in the near-surface layers of a specimen. Edge notches control the

conditions of plastic deformation. There is a correlation between the impact toughness and fracture toughness at equal temperatures. The same mechanism of fracture of ferritic-martensitic steel is observed regardless of the specimen type (including the notches and fatigue cracks).
The regularities of low temperature brittle fracture (crack growth resistance) of the steel at static and dynamic concentrated loads depending on the sizes of Charpy V-Notch (CVN) specimens (standard – ST: 5x10x55 mm, small – SM: 3,3x3,3x30 mm), type of stress concentrators (V-notches with the tip radius of notch r=0,25 mm or a fatigue crack) were investigated in the temperature range from -196 C to +100 C. Impact tests (estimation of KCVN values) were conducted with ST and SM specimens (the energy store 195 J and 50 J). Fracture toughness tests estimating KIC and JIC (static concentrated bending) were conducted with ST specimens (testing machine of "Instron"-type). The following CVN-specimens were tested:
- ST and SM specimens with a one-sided V-notch of 1,5 mm and 1 mm depths, respectively,
- ST specimens with a one-sided V-notch of 1,5 mm depth and two side V-notches of 0,4 mm depth (three-sided V-notch),
- ST and SM specimens with a V-notch and a fatigue crack of 2 mm and 1,2 mm general depth, respectively (one-sided notch with the fatigue crack),
- ST and SM specimens with a V-notch, a fatigue crack and two sided V-notches (three-sided V-notch with the central fatigue crack) as the harshest conditions of the specimen testing.

Some experimental results are shown on the Figs 3-6. Correlations between values of impact toughness and fracture toughness for different specimens and different stress states were found at equal test temperatures. The ductile-to-brittle transition temperatures were determined. The values of DBTT were in the range from -85 C to +35 C depending on the type of CVN-specimens (ST/SM) and stress states (fatigue crack, central and side V-notches). The most impact on the DBTT value at SM specimens testing has "harshness" of the stress concentrators. Such impact for ST specimens is not so strong. There were no shear lips for CVN-SM/ST specimens with the fatigue crack and two side V-notches in the whole investigated temperature range.
The results for the impact toughness of SM/ST specimens with different stress concentrators were compared to the fracture toughness JIC. Linear correlations were observed at equal temperatures. The values of impact toughness and fracture toughness are significantly different for ST and SM specimens. The values for SM specimens are 2.0-2.5 times higher than the corresponding values for ST specimens. This is evidence of significant decrease of the elastic energy store in SM specimens induced by considerable increase of the stress relaxation rate in the crack tip under decreasing of specimen sizes. The work of low temperature fracture of the steel depends on the type of the stress concentrators and specimen sizes and is governed by the elastic energy store and the conditions of plastic deformation in the near-surface layers of the specimens regulated by side notches. One type of fracture mechanism is realized regardless of a specimen type (including notches and a fatigue crack). The marked level of permanent deformation and impact toughness (not less than 3-5 J/sq.cm) was observed at low temperatures (lower than DBTT).

3.1. Fracture toughness after neutron irradiation

Neutron irradiation of the specimens of the steel was irradiated in fast reactor BOR-60. The irradiation temperature was 340 °C and radiation damage 15 dpa (fig. 7). The influence of the type of the thermal treatments (traditional or cyclical) was also investigated. Microstructures steels after different thermal treatment conserve their influences after neutron irradiation and after postradiation annealings (fig. 7).

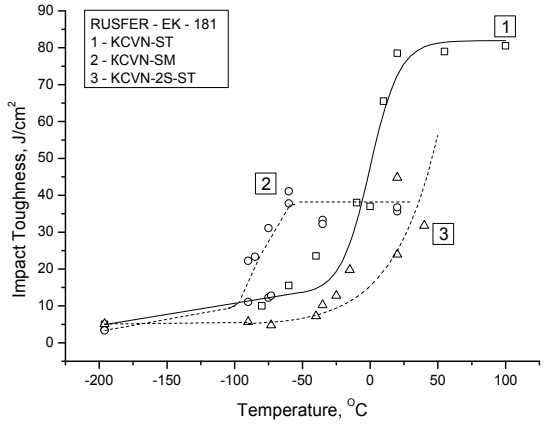

FIG. 3. Temperature dependence of the impact toughness for standard (ST) and small (SM) specimens with the following stress concentrators: (1) KCVN-ST, (2) KCVN-SM, and (3) KCVN-2S-ST.

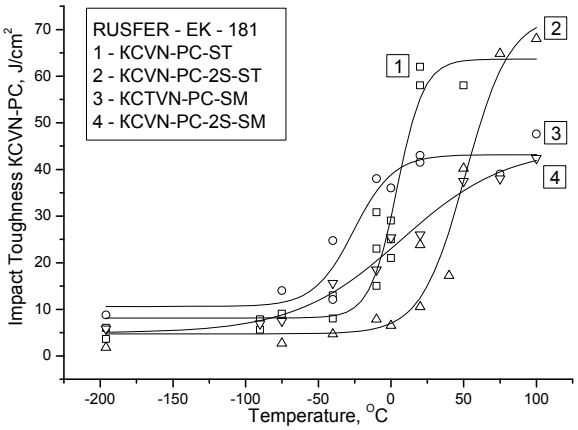

FIG. 4. Temperature dependences of the impact toughness for standard (ST) and small (SM) specimens with the following stress concentrators: (1) KCVN-PS-ST, (2) KCVN-PC-2S-ST, (3) KCVN-PC-SM,(4) KCVN-PC-2S-SM.

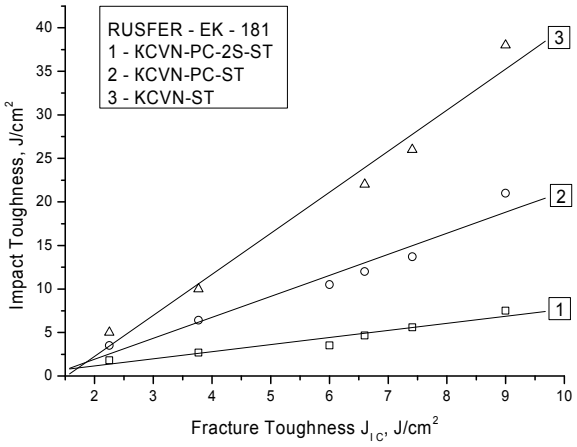

FIG. 5. Relationships between the impact toughness of standard specimens (1) KCVN-PC-2S-ST, (2) KCVN-PC-ST, and (3) KCVN-ST and their fracture toughness J_{1c} at the same test temperature.

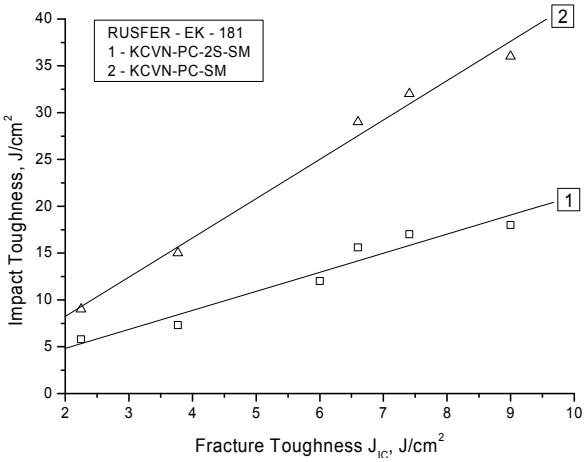

FIG. 6. Relationships between the impact toughness of small specimens (1) KCVN-PC-2S-SM and (2) KCVN-PC-SM and their fracture toughness J_{1c} at the same test temperature.

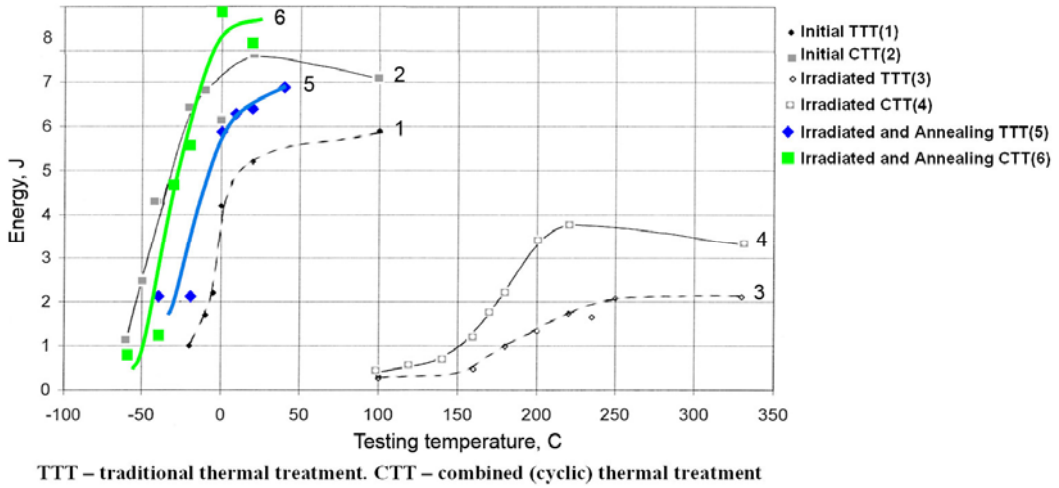

TTT – traditional thermal treatment. CTT – combined (cyclic) thermal treatment

FIG. 7. RUSFER-EK-181: Influence of low-temperature irradiation in BOR-60 reactor (340 C, 15 dpa) on fracture energy at impact test (SSTT). Post irradiation annealing.

4. Multiscale modeling of self-point defects diffusion in iron crystal with dislocations

Diffusion characteristics of self-point defects (vacancies and interstitial atoms) in iron crystal with dislocations of different types were calculated by the methods of multiscale modeling (kinetic Monte Carlo, anisotropic theory of elasticity) in the temperature range from room temperature to 1000 K. The efficiencies of the edge and screw dislocations as point defect sinks governing the heat resistance (dislocation creep) and radiation resistance of the metal were obtained.

Stress fields of dislocations, the basic source of internal stresses, considerably affect the kinetic behavior of self-point defects (SPDs) including their diffusion and absorption by dislocations. Such processes depend on the symmetry of crystal lattices, elastic anisotropy of crystals and the type of crystal defects. Using of multiscale modeling approach enables one to calculate the dislocation sink efficiencies taking into account the factors mentioned above.

Formation energies, dipole-force tensors and diffusivities of SPDs in the absence of the dislocation stress fields were calculated [8,9] in Fe by the molecular statics and molecular dynamics methods. The stable self-interstitial atom (SIA) configuration is the <110> dumbbell. The SIA migration mechanism with the lowest migration energy (0.25 eV) is the <110> dumbbell jump to the nearest lattice sites with a 60° rotation of the dumbbell axis. The vacancy migration mechanism with the lowest migration energy (0.73 eV) is the jump to the nearest lattice sites.

The dislocation stress fields and interaction energy between the SPDs (elastic dipoles) in stable and saddle point configurations and straight edge (ED) and screw (SD) dislocations in slip systems <111>{110}, <111>{112}, <100>{100}, <100>{110} were calculated [2] in the framework of the anisotropic theory of elasticity. At distances less than ~a, it is necessary to use additionally atomistic models. The interaction energies are accurately described by the anisotropic theory of elasticity at distances $\geq 3a$ [9].

The influence of interactions between dislocations and SPDs on the dislocation sink efficiencies for vacancies and SIAs was studied [9] by the object kinetic Monte Carlo (OKMC) method. The probabilities, p_i, for migration jumps in different directions are calculated using Arrhenius frequencies for thermally activated events. There is only one SPD at a time and one dislocation in the simulation box. SPDs starting positions are assigned randomly in the simulation box. The simulation box is a right-angle prism of infinite length with square base (with side length L). The dislocation is situated in the centre of the prism along its axis. Periodic boundary conditions are imposed on the side faces of the simulation box. Thus, a crystal containing a square net of parallel dislocations separated by distance L is simulated. This corresponds to a dislocation density $\rho_d = L^{-2}$. The trajectory of the SPD is followed until it is absorbed by a dislocation at capture radius r_c. After that a new SPD of the same type is introduced into the simulation box. The sink efficiency is then defined as $\xi = k^2/\rho_d = 6 \cdot L^2/\left(l^2 \cdot \langle N \rangle\right)$, where k^2 is the sink strength, l the jump distance ($l = a\sqrt{3}/2$), $\langle N \rangle$ the average number of jumps performed by the SPDs before being absorbed at the sink. At least 10^5 trajectories for each condition have been calculated to obtain a statistically reliable value of the sink efficiency. The inaccuracy of the simulation data is less than 1%. The value of r_c was chosen to be $3a$ as the dislocation core radii in Fe do not exceed this value [9]. The value of L was chosen to be $200a$. Then ρ_d equals ~ $3 \cdot 10^{14}$ m^{-2} in the simulation box which corresponds to a typical value of ρ_d in deformed or irradiated metals. The influence of dislocation elastic fields on the migration energies of SPDs near the simulation box boundaries is less than the value of k_BT at $T = 293$ K at given value of L [9]. Therefore only the interaction of the SPDs with the dislocation in the simulation box was taken into account and all the interactions with image dislocations were considered negligible.

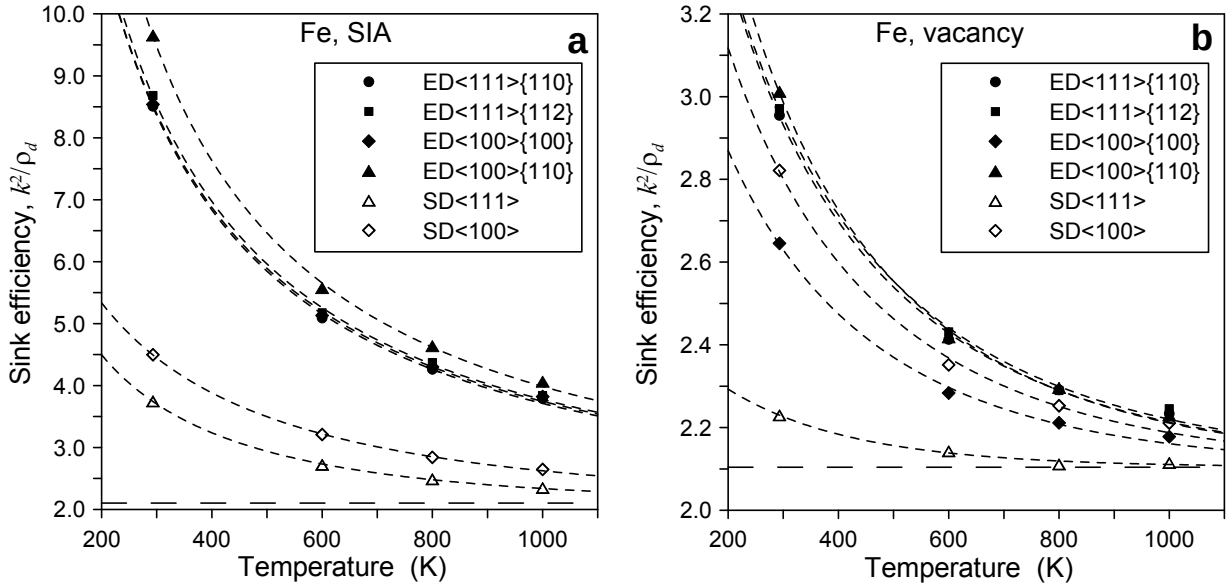

FIG. 8. Temperature dependences of dislocation sink efficiencies. Dashed straight lines mark the value of the linear sink efficiency without elastic interaction with SPDs. (a) Fe, SIA; (b) Fe, vacancy.

The sink efficiency without elastic interaction with SPDs, ξ_0, equals 2.104 at given values of r_c и L. Simulation of SPDs diffusion to dislocations at different temperatures have shown the influence of the elastic fields of dislocations on their sink efficiencies is significant (fig. 8). The sink efficiencies decrease with increasing temperature and tend to the limit ξ_0. Dashed curves at fig. 8 are fits of the simulation data by $\xi(T) = \xi_0 / \left[1 - A \cdot \exp(-B \cdot T)\right]$, where A, B are fitting parameters. The sink efficiencies of EDs are significantly higher (1.5-2.5 times for SIAs) than those of SDs. The exception is SD<100> dislocations for which the sink efficiency for vacancies is comparable to that for EDs (Fig. 8b). All dislocations are more efficient sinks for SIAs than for vacancies. The difference of the sink efficiencies for SIAs and vacancies can be characterized by the bias factor, $B = 1 - \xi_{vacancy} / \xi_{SIA}$, where ξ_{SIA}, $\xi_{vacancy}$ are the sink efficiencies for SIAs and vacancies, respectively. The bias factor decreases with temperature increase for all dislocations. The greatest decrease of B is demonstrated by SD<111> dislocations. The bias factor of SD<111> dislocations at $T = 1000$ K equals 10%, and the analogous value for ED<111>{110} is 41%. The bias factor weakly depends on the slip system of EDs. Its value for EDs with **b** = <100> is 5-10% greater than that for EDs with **b** = ½<111>.

5. Nuclear and Physical Properties of the Steel

On the base of Russian nuclear complex ACDAM [7] radiation damage (dpa), nuclear transmutation changes of the chemical composition, H and He nuclear generation, activation and cooling of the steel were calculated for the long-term irradiation in neutron spectrum of the fusion reactor DEMO-RF (the project of "Kurchatov institute"). Some results are shown on the figs. 9-10.

An important role of correct accounting of all alloying and impurity elements in the elemental composition of the steel in the accurate calculations of the nuclear transmutation, activation, gas accumulation, and cooling has been shown.

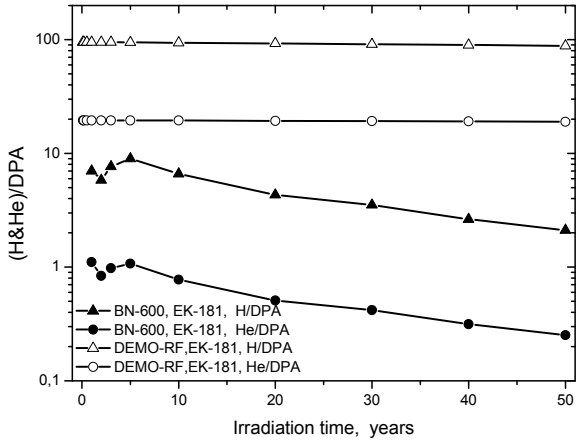

FIG. 9. The irradiation time dependence of H/DPA and He/DPA for ferritic-martensitic steel (RUSFER-181) under the irradiation in BN-600 and DEMO-RF reactors.

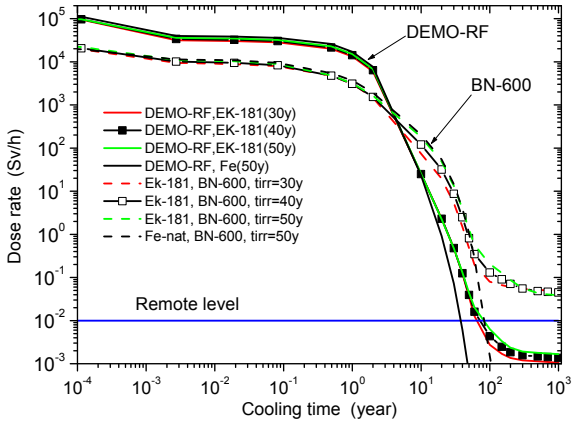

FIG. 10. The dose rate dependence of cooling time for ferritic-martensitic steel RUSFER-181 and pure natural iron (Fe) under the irradiation in BN-600 and DEMO-RF reactors during 30,40 and 50 years.

Element boron significantly increases gas accumulation of helium under irradiation in fission reactor. The influence of boron on the nuclear accumulation of helium is not so significant for fusion reactor comparing to fission reactor. It is also important to take into account the content of nitrogen in the initial steel composition as this content significantly affect accumulation of hydrogen and C-14 isotope for neutron fields of fission reactor. RUSFER-EK-181 steel satisfies well the criterion of low activation (time of achieving the level of 10.00 mSv/hour is significantly lower than 100 years) after irradiation during 50 years in DEMO-RF reactor.

Obtained results give a consistent picture of dynamics of nuclear physical behavior of the ferritic-martensitic steel RUSFER-EK-181 (Fe-12Cr-2W-V-Ta-B) under long-term irradiation (up to 50 years) in the neutron spectra of fission and fusion reactors.

6. BN-600 Experiment

To research the high dose and high temperature properties the BN-600 experiment has been started (April 2010). The results of this experiment will be the radiation properties of the steel RUSFER-EK-181 up to 80 dpa (2012) and up to 160 dpa (2014) and for the irradiation temperatures 370 – 700 C. The rates of the primary radiation damage in the steel and pure iron for the fast (BN-600) and fusion (DEMO-RF) were calculated via complex ACDAM:

Materials	BN-600, dpa/year	DEMO-RF, dpa/year
RUSFER-EK-181	60.75	15.27
Fe (nat)	60.09	15.20

7. Conclusion

(1) We studied the impact toughness and fracture toughness of planar Charpy specimens with a V-shaped notch (CVN specimens) made of a high-temperature ferritic-martensitic steel RUSFER-EK-181 (Fe-12Cr-2W-V-Ta –B) as function of the test temperature (from -196 to +100 C), the specimen dimensions (standard (5*10*55-mm) and small (3.3*3.3*10-mm) specimens), and the type and geometry of stress concentrators (one-and three-sided V-shaped notches with r = 0.25 mm, fatigue crack).

(2) We plotted the temperature dependences of the impact toughness for each type of specimens and determined their ductile-brittle transition temperatures T_{dbtt}. The values of T_{dbtt} fall in the range from -85 to +35 C depending on the state of stress (fatigue crack, lateral V-shaped notches).
(3) We determined the temperature dependences of stress-intensity factor K_{1c} and fracture toughness J_{1c} using concentrated bending tests of standard planar specimens.
(4) The severest type of impact toughness is represented by tests of CVN specimens with an additional fatigue crack and two lateral V-shaped notches(three-sided V-shaped notch with a central fatigue crack,CVN-PC-2S specimens). Under these test conditions, T_{dbtt} is +35 ^{O}C for standard specimens and 0 ^{O}C for small specimens.
(5) The fracture energy of the steel depends on the type of stress concentrator and the specimen dimensions and is determined by the elastic energy and the plastic deformation conditions in the near-surface layers of specimen, which are controlled by lateral notches.
(6) At the same test temperature, the impact toughness J_{1c} are interrelated. Irrespective of the type of specimens (including notches and a fatigue crack) the ferritic-martensitic steel exhibits the same fracture mechanism.
(7) The ductile characteristics of low-temperature fracture of a high-resistance chromium (12%) RAFMS RUSFER-EK-181 (Fe-12Cr-2W-V-Ta-B) demonstrate that it represents a structural material with good resistance to low-temperature brittleness (fracture). At all low temperatures (below T_{dbtt}), a noticeable level of residual ductility (no less than 3-5 J/cm^2) was detected.
(8) The multiscale model developed and the calculation results (using bcc iron as an example) form the basis for further construction and development of the models of formation and evolution of the microstructure (dislocation formation and climb) and properties (heat resistance, swelling, creep, etc.) of metals under various external (radiative, thermal, and mechanical) effects.
(9) Obtained data for functional properties of the RAFMS RUSFER-EK-181 characterize it as the nanostructured structural steel with a good heat resistant (up to 700 C), good resistance to low temperature embrittlement, sufficient radiation resistance of the chemical composition and the structure and phase state. Today recommendations for the temperature window of the steel application are 300 – 670(700) C, and for the advanced (more optimized composition, lower impurity concentrations and thermal treatments) are <300 – 700 C.

References

[1] Klueh R.L., Nelson A.T. 2007, J. Nucl. Mater. 371 37-52,
[2] Baluc N., Abe K., Chernov V.M., et al, 2007, Nucl. Fusion, 47 S696-S717,
[3] Chernov V.M., Leonteva-Smirnova, Potapenko M.M., et al, 2007, Nucl. Fusion 47, p. 839-848
[4] Leonteva-Smirnova M.V., et al, 2006, Perspectivnye Materialy, v. 6, p.40-52 (in russian).
[5] Blokhin D.A., Leonteva-Smirnova M.V., Chernov V.M., et al, 2010, Perspectivnye Materialy, v. 4, p. 26-33 (in russian).
[6] Chernov V.M., Ermolaev G.N., Leonteva-Smirnova M.V. 2010, Technical Physics, Vol. 55, No 7, pp. 985-990.
[7] Blokhin A.I., Demin N.A., Manokhin V.N., et al, 2010, Perspectivnye Materialy, v. 2, p. 46-55 (in russian). See also : Blokhin A.I., Demin N.A., Manokhin V.N., et al, J. Inorganic Materials:Applied Research, 2010, v.1(4), p.311-319.
[8] Sivak A.B., Chernov V.M., Romanov V.A., 2009, Perspektivnye Materialy, v.6, p. 5-11 (in russian)..
[9] Sivak A.B., Romanov V.A., Chernov V.M., Crystallography reports 55(1) (2010) 97-108.